Total electron yields and stopping power of protons colliding with NaCl-type insulator surfaces

Andrea J. García and J. E. Miraglia
Instituto de Astronomía y Física del Espacio, Consejo Nacional de Investigaciones Cientificas y Técnicas, Departmento de Fsica, Facultad de Ciencias Exactas y Naturales. Universidad de Buenos Aires, Casilla de Correo 67, Sucursal 28 (C1428EGA) Buenos Aires, Argentina
(Received 20 October 2006; published 30 April 2007)

In this paper we report electron yields and stopping power of protons colliding with surfaces of NaCl-type insulators formed with the alkali-metal ions Li^+, Na^+, K^+, and Rb^+ and the halides F^-, Cl^-, Br^-, and I^-. We also report fitted models for the static and dynamic polarization potentials of the eight ions of interest. The calculations are carried out within the shellwise local plasma approximation using the Levine-Louie response function, instead of the usual Lindhard one, to account for the ionization energy.

DOI: 10.1103/PhysRevA.75.042904 PACS number(s): 34.50.Bw, 34.50.Dy, 79.20.−m

I. INTRODUCTION

When a fast proton impacts on a crystal surface with a grazing angle, it excites target electrons to the continuum. Two relevant quantities can be measured, *viz.*: the number of emitted electrons, generally called the yield, and the energy lost by the projectile or the stopping power (for comprehensive reviews on the subject we refer to Refs. [1,2]). In more detailed experiments, both measurements are taken in coincidence [3,4]. We are particularly interested in calculating the yield and stopping of protons colliding with NaCl-type insulator surfaces.

The physics of the process is governed by two major aspects of the collision: the projectile trajectory and the differential probability of inelastic transition at every segment of the collision.

In a previous article [5] we have used the shellwise local plasma approximation (SLPA), which let us evaluate not only the probability but the polarization potentials. In that article, we considered the LiF target and used the well-known Lindhard dielectric function to describe the local plasma. This choice has a setback: inelastic transitions are permitted for energies below the ionization energies of the ions composing the crystal. To fix this problem we could cut off the forbidden energies and so violate the Kramers-Krönig relation. In this paper, we resort instead to the more elaborate Levine-Louie dielectric response function [6]. This response can account for an energy gap without losing important properties such as the *f*-sum rule and the Kramers-Krönig relation. Accordingly, the polarization potentials as well as differential probabilities are calculated on equal footing.

As in a previous paper, to describe the electronic density of the ions forming the lattice we use a simple atomic model called GII (grid of independent ions), which allows us to use the well-known Hartree-Fock wave functions.

In synthesis, the basic considerations we assume are as follows:

(1) The insulator surface is considered to be composed by an array of alkali-metal ion and halide ions at the places given by the crystal parameters, and the local electronic density is described by the Hartree-Fock wave functions of the isolated ions. This is what we call the grid of the independent ion (GII) model.

(2) The polarization potentials as well as differential probabilities are calculated accordingly using the Levine-Louie response function where the gap, in accordance with the GII model, is considered to be the ionization energy of the isolated ion.

(3) The trajectory of the projectile is calculated classically considering the interaction (static and dynamic polarization) within the planar model.

(4) The stopping power and the electron yield are calculated at each segment of the collision along the classical projectile trajectory.

In this paper we report a complete set of electron yields and stopping power of protons colliding grazingly with sixteen NaCl-type insulator surfaces built with the four alkali-metal ions Li^+, Na^+, K^+, and Rb^+ and the four halides F^-, Cl^-, Br^-, and I^-. Also, in Table I below, we report fittings for the static and dynamic polarization potentials of the eight ions of interest. In Sec. II, we calculate the polarization potentials and in Sec. III we present the results. Atomic units are used unless otherwise indicated.

II. PROJECTILE-ION POTENTIALS

We consider two different contributions to describe the interactions of the projectile with each target ion: the *static* and the *polarization* potentials, V_{st} and V_{pol}^{LL} below. The total potential is simply the sum $V=V_{st}+V_{pol}^{LL}$. The superscript + and − will be used to individualize the interaction with the alkalide and halide, respectively.

A. Static potentials

The *static* potential is simply the potential created by ion targets considering that the electronic cloud rests *frozen*. The static potentials, $V_{st}^{+}(r)$ and $V_{st}^{-}(r)$ for alkali-metal ions and halide, respectively, can be expressed as follows:

$$V_{st}^{\pm}(r) = \pm\frac{1}{r} + \frac{Z^{\pm}(r)}{r}, \tag{1}$$

$$Z^{+} \to \begin{cases} Z_T^{+} - 1, & r \to 0 \\ 0, & r \to \infty, \end{cases} \qquad Z^{-} \to \begin{cases} Z_T^{-} + 1, & r \to 0 \\ 0, & r \to \infty, \end{cases} \tag{2}$$

where Z_T^{+} (Z_T^{-}) is the target nuclear charge of the alkali-metal ion (halide) and r is the position of the projectile with respect

 ©2007 The American Physical Society

TABLE I. Atomic coefficients for halide and alkalide ions.

Ion	$\langle r^2\rangle$	R_a^2	$\langle r^3\rangle$	R_b	N	V'_∞	α'_∞	(Z_1,Z_2,Z_3)	(μ_1,μ_2,μ_3)
I^-	7.79	8.273	27.86	3.20	6	158	250	(23.21, 26.10, 4.69)	(1.443, 5.900, 26.66)
Br^-	5.72	6.113	18.18	3.10	6	132	158	(9,889, 22.922, 3.189)	(1.087, 4.103, 23.98)
Cl^-	4.56	4.590	13.34	3.00	6	115	111	(10.167, 7.548, 0.2845)	(1.199, 5.985, 44.40)
F^-	1.98	1.898	4.41	2.70	6	68.5	35	(2.063, 7.023, 0.914)	(1.824, 1.834, 16.05)
Rb^+	3.21	3.582	7.00	1.95	6	50.7	70	(10.579, 22.303, 3.118)	(1.458, 4.487, 25.36)
K^+	2.28	2.610	4.315	1.78	6	41.7	48	(11.416, 6.172, 0.412)	(1.765, 7.426, 26.56)
Na^+	0.795	0.713	0.977	1.40	5.5	22.2	10	(0.496,8,969,−0.535)	(2.738, 2.784, 26.18)
Li^+	0.445	0.369	0.439	1.15	5	4.64	1.5	(−0.114,2.492,−0.378)	(1.753, 3.711, 9.961)

to one lattice ion. From basic definitions, the Hartree-Fock approximation produces

$$Z^{\pm}(r) = \sum_{nl} r \int d\mathbf{x} \frac{|\varphi_{nl}^{\pm}(x)|^2}{|\mathbf{r}-\mathbf{x}|}, \tag{3}$$

where $\varphi_{nl}^{\pm}$ are, in our case, the anion and cation wave functions [7]. As in Ref. [5], we have fitted $Z^{\pm}(r)$ as a combination of simple exponentials

$$Z^{\pm}(r) \cong Z_{fit}^{\pm}(r) = \sum_{j=1}^{3} Z_j^{\pm} \exp(-\mu_j^{\pm} r). \tag{4}$$

A list of the parameters $Z_j^{\pm}$ and $\mu_j^{\pm}$ for the eight ions are displayed in Table I. For the fitting procedure we have started with seed values for Z_j and μ_j given by those of the Moliere potential. These values are the best we can attain considering the structure of Eq. (4), and they replace the more general ones given by Moliere or the Ziegler-Biersack-Littmark (ZBL) expression [8].

B. Polarization potential

First, let us start recalling the *static polarization* potential. It is due to the distortion of the cloud induced by a charge at rest. In its usual form [9,10], it reads

$$V_{sp}(r) = -\frac{\alpha_0}{2(R_0^2+r^2)^2}, \tag{5}$$

where α_0 is the well-known *static* or electric-dipole polarizability and R_0 is a cutoff. It is generally related to the radius of the shell $R_0^2=\langle r^2\rangle$. In general, we define $\langle r^i\rangle = 0.75\langle r^i\rangle_{np^6} + 0.25\langle r^i\rangle_{ns^2}$. Values of $\langle r^i\rangle$ for $i=2$ and 3 are displayed in Table I. The value of α_0 has been calculated with a high degree of precision for most of the neutral atoms and ions. Polarizability values for the ions of interest can be found in Refs. [11–14].

For large velocities we can no longer consider the static term but the *dynamic* polarizability, which depends on the impact velocity v. To introduce the dynamic polarizability of the target, we resort to the self-energy induced by a moving charge in a free-electron gas. We first introduce the dynamic self-induced potential as

$$V^{SLPA}(r) = -\frac{1}{2\pi v}\sum_{nl}\int_0^{\infty} d\omega \int_{w/v}^{\infty} dq\, \mathrm{Re}[W_{nl}(q,\omega,r)], \tag{6}$$

$$W_{nl}(q,\omega,r) = \frac{2Z_P^2}{\pi v}\frac{1}{q}\left[\frac{1}{\varepsilon(q,\omega,k_{Fnl}(r))} - 1\right], \tag{7}$$

where $k_{Fnl}(r)$ is the space-dependent Fermi velocity, $k_{Fnl}(r)=[3\pi^2\rho_{nl}(r)]^{1/3}$, $\rho_{nl}(r)$ is the electron density of the nl state $\rho_{nl}(r)=|\phi_{nl}(r)|^2$, and $\phi_{nl}(r)$ are the bound-state wave functions given in the tables of Ref. [7]. In Eq. (7), $\varepsilon(q,\omega,k_{Fnl})$ is the dielectric response function.

In Ref. [5], we have used the well-known Lindhard dielectric function $\varepsilon^L(q,\omega,k_{Fnl})$. This choice has a setback: inelastic transitions are permitted for energies below the ionization energies corresponding to the corresponding electronic state. To cut off this forbidden region we resort to the Levine-Louie dielectric-response function $\varepsilon^{LL}(q,\omega,k_{Fnl})$ [6] defined as follows:

$$\mathrm{Im}\,\varepsilon^{LL}(q,\omega,k_{Fnl}) = \begin{cases} \mathrm{Im}\,\varepsilon^L(q,\tilde{\omega},k_{Fnl}), & \omega > \omega_g \\ 0, & \omega < \omega_g, \end{cases} \tag{8}$$

where the energy shift $\tilde{\omega}^2=\omega^2-\omega_g^2$ has been introduced. In accordance with our independent ion model we consider $\omega_g=|\varepsilon_{nl}|$, but any other experimental value representing the band gap could have been used. Accordingly, and this is a very important point, in this case we would need to know the corresponding state functions providing those gaps to be used in the definition of the local Fermi velocity. In this sense, our proposal is fully coherent: we use the proper function, which produces the ionization binding energy of the isolated ion.

Once the imaginary part is obtained, the real part, $\mathrm{Re}\,\varepsilon^{LL}(q,\omega,k_{Fnl})$, is obtained through the Kramers-Krönig relation. After some algebra we find that for $\omega>\omega_g$ $\mathrm{Re}\,\varepsilon^{LL}(q,\omega,k_{Fnl})=\mathrm{Re}\,\varepsilon^L(q,\tilde{\omega},k_{Fnl})$, while for $\omega<\omega_g$ a closed form can be obtained. (For details see Ref. [6].)

$$\mathrm{Re}\,\varepsilon^{LL}(q,\omega,k_{Fnl}) = 1 + \frac{2}{\pi k_F}\left(k^2 + \frac{D}{2}k^3A + B\right), \tag{9}$$

$$A = \arctan\frac{X_+}{D} + \arctan\frac{X_+}{D}, \quad X_{\pm} = \frac{2}{k} \pm \frac{1}{k^2}, \tag{10}$$

$$B = \left(\frac{D^2}{8}k^5 + \frac{1}{2}k^3 - \frac{1}{8}k\right)\ln\frac{D^2 + X_+^2}{D^2 + X_-^2}, \tag{11}$$

$$D = \frac{\omega_g}{\omega_F}\sqrt{1 - \frac{\omega^2}{\omega_g^2}}, \quad k = \frac{q}{k_F}, \quad \omega = \frac{1}{2}k_F^2, \tag{12}$$

and in our case $\omega_g = |\varepsilon_{nl}|$. One can immediately prove that ε^{LL} satisfies the f-sum rule and for $\omega < \omega_g$ plasmon excitation cannot take place. Replacing $\varepsilon^{LL}(q, \omega, k_{Fnl})$ in Eqs. (7) and (6), we obtain the ionization-gap-corrected version of the potential that we call $V_{pol}^{LL}(v, r)$.

It will be important for the discussion below to define the integrated value

$$\langle V_{pol}^{LL}\rangle = \int d\mathbf{r}\, V_{pol}^{LL}(v, r). \tag{13}$$

From numerical calculation we observe that the following limits hold:

$$\langle V_{pol}^{LL}\rangle \to \begin{cases} V'_\infty/v & \text{for } v \to \infty \\ V'_0 & \text{for } v \to 0. \end{cases} \tag{14}$$

Results for V'_∞ are presented in Table I for the eight ions.

As in Ref. [5], we found it convenient to use a fitting $V_{fit}^{LL}(v, r)$ to describe $V_{pol}^{LL}(v, r)$. The most suitable was

$$V_{fit}^{LL}(v, r) = -\frac{\alpha'(v)}{2[R_0^2 + r^2 + (r/R_b)^N]^2}, \quad R_0^2 = R_a^2\beta(v). \tag{15}$$

For most of the cases $N=6$ (except for anomalous cases Na^+ and Li^+, where the best values are $N=5.5$ and 5, respectively). A list of the best values for R_a and R_b are shown in the table. To find this set of values, two conditions were imposed.

(i) The $\lim_{v->\infty} R_0^2 = R_a^2$ (or $\lim_{v->\infty}\beta = 1$), and

(ii) $\int d\mathbf{r} V_{fit}^{LL}(v, r) = \langle V_{pol}^{LL}(v)\rangle$.

In this way we determine R_a^2 and β. We can observe that $\langle r^2\rangle_{ns^2} < R_a^2 < \langle r^2\rangle_{np^6}$ and R_a^2 differs from $\langle r^2\rangle$ in less than 10% (see Table I). β dependences on the velocity for the eight ions are displayed in Fig. 1.

Note that for $r < R_c = R_b^{N/(N-2)}$, $V_{fit}^{LL}(v, r)$ has a structure equal to the static polarization potential $V_{sp}(r)$ given by Eq. (5). For $r > R_c$, V_{fit}^{LL} falls sharply as $\alpha'(R_b/r)^{2N}$ and it becomes independent from the product $R_a^2\beta$.

The limits of α' with the velocity were found to be

$$\alpha'(v) \to \begin{cases} \alpha'_\infty/v & \text{for } v \to \infty \\ \alpha'_0 & \text{for } v \to 0. \end{cases} \tag{16}$$

Strength dependence on the inverse velocity value seems to be very good for $v \geq 1$ for all the cases, and for $v \geq 2$ for the anomalous cases (Na^+ and Li^+). At small distances, $V_{pol}^{LL}(v, r)$ cannot be well fitted, but in this case the static potential is dominant and this flaw can be disregarded. Otherwise, the fitting is quite accurate. All possible cases are shown in Fig. 2 where the polarization potentials are plotted for eight ions and for several proton impact velocities.

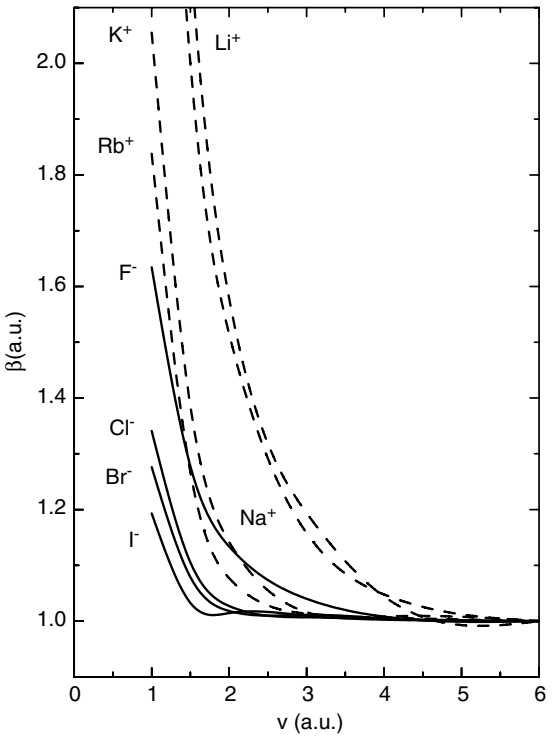

FIG. 1. Parameter β as a function of the ion velocity for the eight ions of interest.

C. Scrutinization of the polarization potentials

We have summed up the fitting to the dynamic polarization potential to the parameters, α'_∞, R_a^2, R_b, and N which can be obtained from Table I, and $\beta(v)$, which can be extracted from Fig. 1. We are now ready to test the reliability of our model to describe the polarization.

First, according to Clausius Mossotti's simple model, it is well known that the polarizability is expected to be proportional to the volume of the atom. The static polarizability α_0

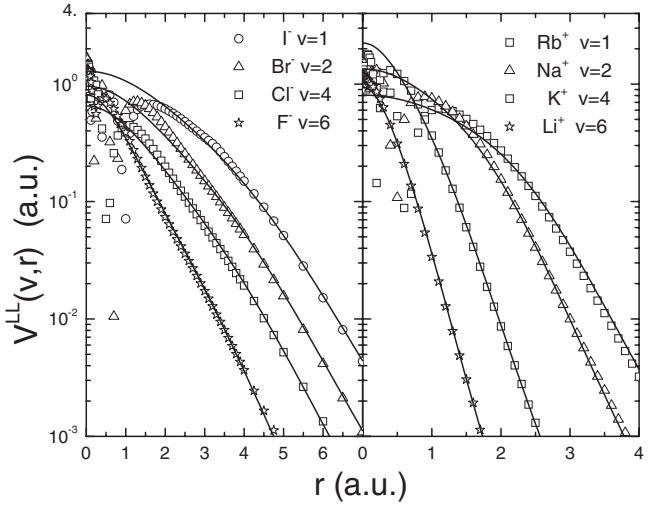

FIG. 2. Plots of the polarization potentials V_{pol}^{LL} and their fittings V_{fitt}^{LL} as given by Eq. (15) for the eight ions of interest for different velocities.

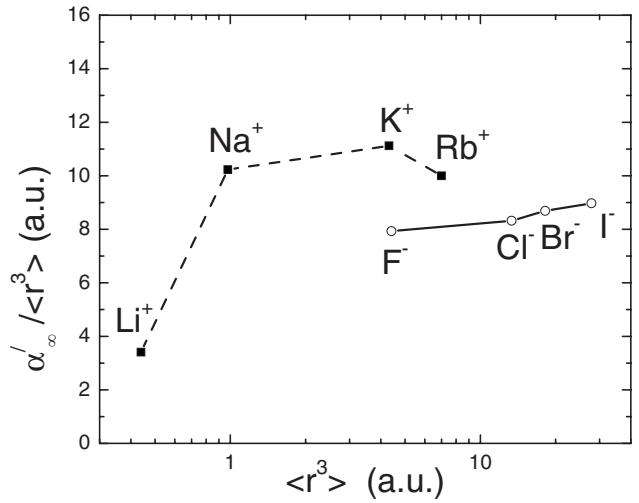

FIG. 3. Plot of the polarization terms $\alpha'_\infty/\langle r^3\rangle$ as a function of $\langle r^3\rangle$ for the eight ions of interest. Values for α'_∞ and $\langle r^3\rangle$ are given in Table I.

is then expected to be roughly linearly proportional to $\langle r^3\rangle$. Following this line, in Fig. 3 we plot the ratio $\alpha'_\infty/\langle r^3\rangle$, which turns out to be nearly constant (except again for the Li^+ anomalous case). This encouraging finding seems to indicate that the fitting procedure is appropriate.

Second, using the wake theory within the random-phase approximation (RPA) dielectric response function of an electron gas one can prove that the self-induced potential at the projectile position of a Coulomb at large velocities is given by (see Eq. (9.9) of Ref. [15])

TABLE II. Experimental and theoretical plasmon values and critical angles for different velocities.

	ω_p (eV)		Θ_c (deg)			
Crystal	exp	ω'_p	$v=2$	$v=3$	$v=4.47$	$v=6.32$
LiF	26	31.2	0.84	0.60	0.42	0.31
LiCl	18	24.6	0.97	0.67	0.47	0.34
LiBr	16.3	22.8	1.15	0.79	0.54	0.39
LiI	13.3	20.9	1.27	0.86	0.59	0.42
NaF	20.1	25.5	0.94	0.65	0.45	0.33
NaCl	15.7	21.2	1.00	0.69	0.48	0.34
NaBr	14.4	20.1	1.15	0.79	0.54	0.39
NaI	12.8	18.4	1.25	0.85	0.58	0.41
KF	16.8	19.9	1.02	0.70	0.49	0.35
KCl	13.3	17.4	1.04	0.72	0.49	0.36
KBr	12.4	16.7	1.16	0.79	0.52	0.39
KI	11.2	15.6	1.23	0.84	0.57	0.41
RbF	15	18.4	1.19	0.82	0.56	0.40
RbCl	12.4	16.1	1.15	0.79	0.54	0.39
RbBr	11.6	15.7	1.25	0.86	0.58	0.42
RbI	11	14.6	1.30	0.89	0.60	0.43

$$\lim_{r\to 0}\Phi_w = -\frac{Z_P\pi}{4v}\omega_p, \tag{17}$$

where ω_p is the plasmon frequency. Available experimental values of the plasmon energies [16] are displayed in Table II. Within our approach, the total induced polarization could be obtained by integrating all the possible target positions to give Eq. (13). The integrated value $\langle V^{LL}_{pol}\rangle$ should then be compared with Eq. (17). So, for proton impact, we can rewrite

$$\langle V^{LL}_{pol}\rangle = \lim_{r\to 0}\Phi_w = \frac{V'_\infty}{v} = -\frac{\pi}{4v}\omega'_p, \tag{18}$$

and we can estimate ω'_p to give

$$\omega'_p = \frac{4v}{\pi}\langle V^{LL}_{pol}\rangle \simeq \frac{4\alpha'_\infty}{\pi}. \tag{19}$$

In Table II, we display the experimental values of the plasmon energy as compared with the prediction given by Eq. (19). The prediction seems to be reasonably good. The term ω'_p is larger than the experimental value ω_p within the range 16–34 %. A similar estimation using the simple Lindhard dielectric function [5] instead of the Levine-Louie estimation gives a larger overestimation. The reason is based on the contribution of the term given by Eq. (9) not present in the Lindhard case.

III. RESULTS

A. Penetration angle

The calculation of the penetration angle is an important application of the potentials proposed. In the planar model, the critical angle θ_c is calculated assuming a surface density of targets and describing the planar potential $V^\pm_Z(z)$. It depends on the distance z to the surface

$$V^\pm_Z(v,z) = \int d\mathbf{r}\, V^\pm(v,r)\,\delta(\sqrt{z^2+r^2}), \tag{20}$$

where δ is the delta function. The total (central) potential $V^\pm(r)$ includes the static plus polarization terms $V^\pm(v,r) = V^\pm_{st}(r) + V^{LL\pm}_{pol}(v,r)$ and the total planar (potential) reads, $W_Z(v,z) = \delta_s[V^-_Z(v,z) + V^+_Z(v,z)]$, where $\delta_s = \delta^+_s = \delta^-_s$ is the superficial density of ions characterized by the corresponding Miller indices [100]. The critical angle is determined when the kinetic energy K equals the potential at the surface, i.e.,

$$W_Z(v,0) = K = \frac{1}{2}M_P(v\,\sin\,\theta_c)^2. \tag{21}$$

A list of planar critical angles as a function of the velocity is displayed in Table II. For larger velocities, the inverse dependence can be used, i.e., $\theta_c \propto 1/v$. The values are slightly smaller than the ones given by the Moliere potential due to the polarization potential. In the planar model, the projectile rebounds for incident angles $\theta < \theta_c$ and penetrates for $\theta > \theta_c$. For more elaborate models such as the punctual model, it is more appropriate to introduce a percentage of

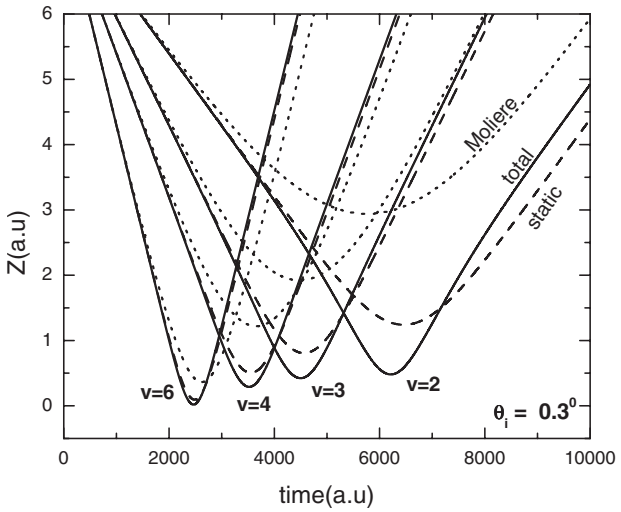

FIG. 4. Proton trajectory on LiF [100] surfaces for four different velocities. Dotted lines result using just the repulsive Moliere potential, dashed lines result using our static potential, and solid lines result using added static and polarization potentials, as done in this paper.

penetration, having a value of 50% near the critical angle [5]. In Fig. 4, we plot proton trajectories colliding with LiF for four velocities, 2, 3, 4, and 6 according to the planar channeling model. The trajectories not only change when we use our static potential—instead of Moliere—but also as we add the polarization potential. The influence of the polarization potential diminishes as we increase the velocity, but at intermediate energies it produces substantial contributions.

B. Stopping and number of emitted electrons

To be coherent with the used potential we also use the Levine-Louie dielectric function to calculate the moments of the energy per unit path dl as well, i.e.,

$$\frac{d\langle\omega^j\rangle(z)}{dl} = \int d\mathbf{r}\ \delta(\sqrt{z^2+r^2}) \sum_{nl} \int_{\omega_g}^{\infty} d\omega\ \omega^j \frac{1}{v} \times \int_{w/v}^{\infty} dq\ \mathrm{Im}[W_{nl}^{LL}(q,\omega,r)], \tag{22}$$

where with W_{nl}^{LL} we have explicitly indicated that the Louie-Levine dielectric-response function is being used in Eq. (7). The first moment is simply the stopping; $d\langle\omega^1\rangle/dl = dS/dl$. The zero order means the inverse number of the mean free path, or, what is equivalent, the number of electrons that undergo inelastic transitions, i.e., $d\langle\omega^0\rangle/dl = d\gamma/dl$ and γ is called the yield. According to our model an inelastic transition means the absorption of energy the electron requires to be ionized. Thus all these electrons end up in a free state to be counted by the detector. Usually, not all the electrons are

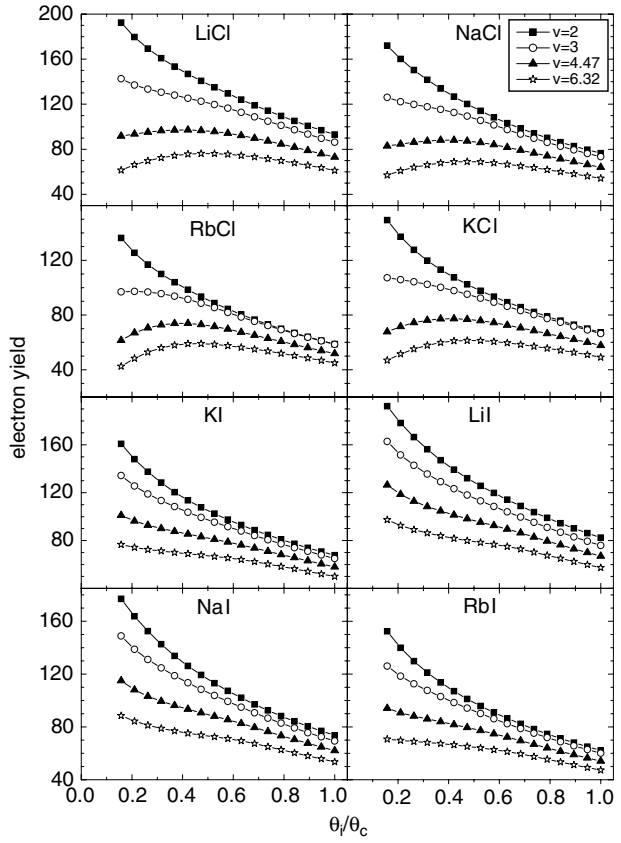

FIG. 5. Number of total electron production (yields) as a function of the proton penetration angle normalized to the critical one (see Table II) for different velocities and insulators as indicated.

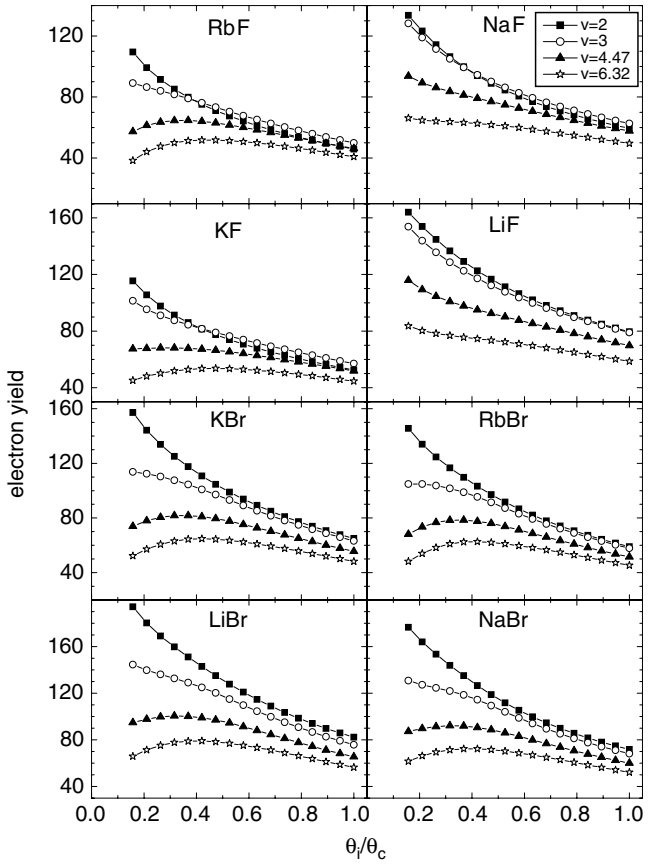

FIG. 6. Same as Fig. 5, for different surface targets as indicated.

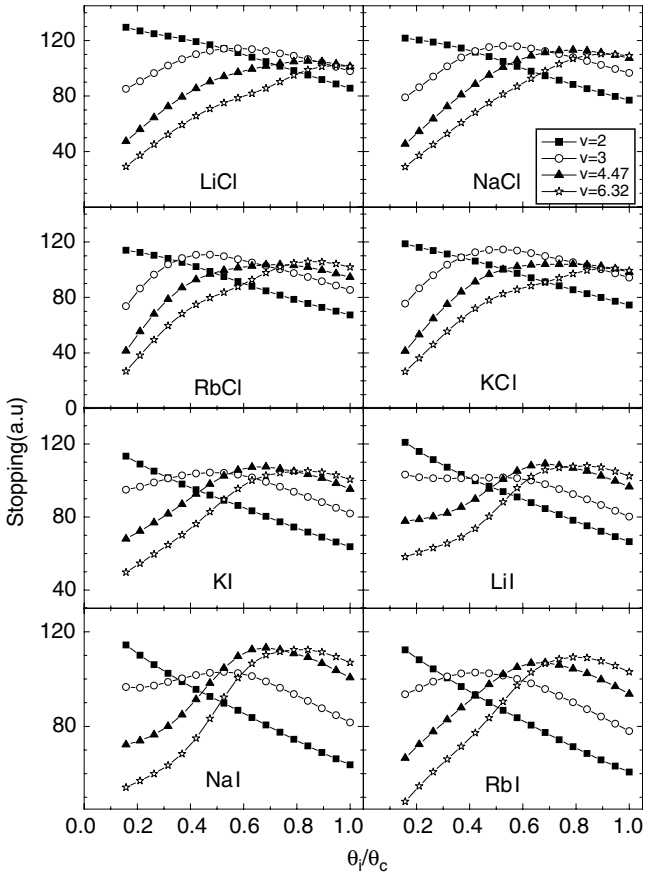

FIG. 7. Stopping power as a function of the proton penetration angle normalized to the critical one (see Table II) for different velocities and insulators as indicated.

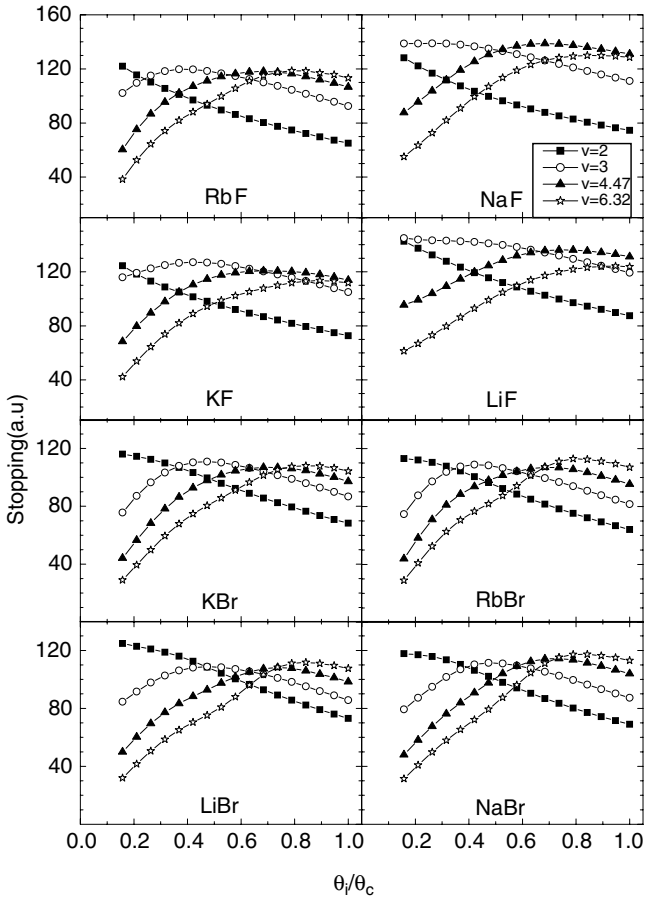

FIG. 8. Same as Fig. 7, for different surface targets as indicated.

detected in the experimental set up but only those that escape to the vacuum. The total electron production is obtained after integrating along the trajectory,

$$\gamma = 2v \int_{Z\,\mathrm{min}}^{\infty} dz \frac{d\langle \omega^0(z)\rangle/dl}{\sqrt{v^2 \sin^2 \theta_i - \frac{2}{M_p} W_Z(v,z)}}, \qquad (23)$$

and similarly for the stopping.

For F^- and Na^+ we have considered the K- and L-shell contributions, for Cl^- and K^+ the L and M, for Br^- and Rb^+ the M and N, and for I^- the N and O shells. The inner-shell vacancies have been accounted twice to the electron production to take into account the additional electron coming from the postcollision autoionization. This contribution is noticeable just at large penetration angles where the projectile probes the inner shell.

With this approach based on the dielectric function of Levine and Louie we tackle the collisions of protons on the sixteen insulators. For a given velocity and incident angle, their calculation requires a four-dimensional integral; three in Eq. (22) and an additional one for the trajectory given by Eq. (23). In addition, the potential $W_Z(v,z)$ requires a further three-dimensional integral [Eqs. (6) and (20)]. In Figs. 5 and 6, we plot total electron production and in Figs. 7 and 8 we plot the total energy loss. The surfaces are considered perfectly plane along the direction (100). In general, the total number of electrons can be estimated in the range $\gamma \in \{40,200\}$ and total stopping, $S \in \{30,150\}$. In this velocity region the numbers (in atomic units) are very roughly in the same order of magnitude $\gamma \sim S$, which seems to mean that the projectile cedes something in the order of an atomic unit of energy per electron ionized.

For the total γ yield, all the curves follow approximately the same pattern; γ decreases with v and θ/θ_c. The situation is quite different for the stopping because it changes shape with the velocity. The larger the velocity and incident angle, the deeper does the projectile probe into shells and the more inelastic collisions are expected to be.

C. Summary and future developments

We have calculated the total electron production and stopping of protons colliding with sixteen ClNa-type insulator surfaces. We expect that comparing these resulting values with a large variety of experimental results will be of great interest. The whole range of ClNa-type insulators were here covered and in a wide scope of experimental activity. Besides the shellwise local plasma approximation, which is the central hypothesis in this paper, we estimate that in general the electron yields presented here underestimate the data for

three reasons. First, the polarization potential is possibly larger than expected in between 16% and 34%, as indicated. The reason is surely that we considered isolated ions with an atomic ionization gap. But had we introduced the crystal Madelung potential, the wave function may have a larger ionization potential (the gap would increase) and surely the polarization potential, would diminish. We have observed that the smaller the polarization potential, the larger the yield, and so a corrected potential would increase the yields slightly, especially at intermediate velocities.

Second, secondary electron emission has been disregarded. Thus primary electrons ejected from a direct collision with the projectile can subsequently collide with target ions, thus producing new electrons, which are experimentally counted, but not calculated here.

And third, the planar model should be improved to account for the punctual channeling, as we developed in Ref. [5]. In all cases, we have observed that the yield and the stopping notably increases, especially at larger incident angles. The only obstacle is the huge computing time. To calculate a total yield using the punctual channeling model, for example, would require a computing time in the order of 10^5 longer than the planar model; an order of 10^3 azimuth angles with respect to [100] direction and 50 initial or more initial conditions are needed to randomize the starting point of the projectile. We are currently optimizing the code to cover the present system. In accordance with our experience with LiF [5] we may expect an increase up to 20% in the electron production near the critical angle.

ACKNOWLEDGMENTS

The authors would like to acknowledge financial support from CONICET, UBACyT, and ANPCyT of Argentina.

[1] H. Winter, Phys. Rep. **367**, 387 (2002).
[2] J. Burgdörfer, *Progress in Atomic and Molecular Physics*, edited by C. D. Lin (World Scientific, Singapore, 1993).
[3] K. Kimura, G. Andou, and K. Nakajima, Phys. Rev. Lett. **81**, 5438 (1998).
[4] G. Andou, K. Nakajima, and K. Kimura, Nucl. Instrum. Methods Phys. Res. B **160**, 16 (2000).
[5] A. J. García and J. E. Miraglia, Phys. Rev. A **74**, 012902 (2006).
[6] Z. H. Levine and S. G. Louie, Phys. Rev. B **25**, 6310 (1982).
[7] E. Clementi and C. Roetti, At. Data Nucl. Data Tables **14**, 177 (1974).
[8] J. F. Ziegler, J. P. Bierzack, and U. Littmark, *The Stopping and Range of Ions in Solids* (Pergamon Press, New York, 1985), Vol. 1.
[9] T. M. Miller and B. Bederson, Adv. At. Mol. Phys. **13**, 1 (1977).
[10] C. J. Joachain, *Quantum Collision Theory* (North Holland, Amsterdam, 1979).
[11] N. W. Grimes and R. W. Grimes, J. Phys.: Condens. Matter **10**, 3029 (1998).
[12] R. D. Shannon, J. Appl. Phys. **73**, 348 (1993).
[13] D. C. Ghosh and R. Biswas, Int. J. Mol. Sci. **4**, 379 (2003).
[14] J. E. Miraglia and M. S. Gravielle, Phys. Rev. A **67**, 062901 (2003).
[15] P. M. Echenique, F. Flores, and R. H. Ritchie, Solid State Phys. **43**, 229 (1990).
[16] V. K. Srivastava, Phys. Rev. B **29**, 6993 (1984).